PERGAMON

Deep-Sea Research II 48 (2001) 1823–1836

DEEP-SEA RESEARCH
PART II

www.elsevier.com/locate/dsr2

Covariation of mesoscale ocean color and sea-surface temperature patterns in the Sargasso Sea

D.J. McGillicuddy Jr.[a,*], V.K. Kosnyrev[a], J.P. Ryan[b], J.A. Yoder[c]

[a]*Department of Applied Ocean Physics and Engineering, Woods Hole Oceanographic Institution, Woods Hole, MA 02543, USA*
[b]*Monterey Bay Aquarium Research Institute, P.O. Box 628, 7700 Sandholdt Road, Moss Landing, CA 95039, USA*
[c]*Graduate School of Oceanography, University of Rhode Island, Narragansett, RI 02882, USA*

Abstract

During the lifetime of the Coastal Zone Color Scanner, there were 21 instances in which both satellite-derived ocean color and sea-surface temperature are simultaneously available over large areas of the Sargasso Sea. These images reveal close correspondence between mesoscale structures observed in temperature and pigment fields. In general, higher (lower) pigment biomass occurs in mesoscale features consisting of cold (warm) temperature anomalies. This relationship is consistent with the idea that upward displacement of isopycnals at the base of the euphotic zone by mesoscale eddies is an important mechanism of nutrient supply in the region.

1. Introduction

It has been recognized for some time that mesoscale processes could have a significant impact on biogeochemical cycling in the upper ocean. Analysis of two hydrographic profiles sampled 1 month apart in the summer of 1986 off Bermuda documented an apparently eddy-driven nutrient injection event that could account for 20–30% of the annual new production (Jenkins, 1988). Since these observations were published, several different lines of evidence have suggested that mesoscale eddies are the dominant mode of nutrient transport in the Sargasso Sea (McGillicuddy et al., 1999). High-resolution regional numerical simulations suggest eddy-induced upwelling causes intermittent fluxes of nitrate into the euphotic zone of magnitude sufficient to balance the nutrient

* Corresponding author. Tel.: + 1-508-289-2683; fax: + 1-508-457-2194.
E-mail address: dmcgillicuddy@whoi.edu (D.J. McGillicuddy Jr.).

0967-0645/01/$ - see front matter
PII: S0967-0645(00)00164-8

demand implied by geochemical estimates of new production (McGillicuddy and Robinson, 1997; hereafter MR97). Nitrate-flux calculations based on satellite altimetry and a statistical model linking sea-level anomaly to subsurface isopycnal displacements provide estimates of comparable order (Siegel et al., 1999). Observations of a nutrient pulse associated with a mesoscale eddy were obtained using novel chemical sensing technology deployed on the Bermuda Testbed Mooring (McNeil et al., 1999). Most recently, mesoscale biogeochemical surveys have been carried out as part of the validation activities of the Bermuda Atlantic Time-series Study (BATS). These observations demonstrate that eddy-induced upward displacement of density surfaces can inject nutrients into the euphotic zone and result in the accumulation of biomass in the overlying waters (McGillicuddy et al., 1999).

Shipboard sampling of this highly intermittent process suffers from some inherent practical limitations. Eddy-resolving biogeochemical surveys can provide three-dimensional snapshots in time, but the effort required to carry them out precludes doing so on a frequent basis. Fixed-point time-series operations such as BATS (Michaels and Knap, 1996) and the Bermuda Testbed Mooring Program (Dickey et al., 1998) have yielded important clues about the nature of these phenomena. However, one-dimensional observations simply do not fully resolve this fundamentally three-dimensional process (Doney, 1996). Satellite-based remote sensing offers the only observational approach suitable for routine synoptic measurement of physical and biological properties over large regions of the ocean. Of course, such technology is not without its own limitations. For example, satellite ocean color and SST are limited to near-surface distributions and contain no information about vertical structure, and both require cloud-free viewing of the ocean surface. Nevertheless, these data provide a window into space and time-scales that are not accessible with any other type of observation.

Archived data from the Coastal Zone Color Scanner (CZCS) and Advanced Very High Resolution Radiometer (AVHRR) instruments afford an excellent opportunity to investigate mesoscale variations in ocean color and sea-surface temperature (SST). Previous investigations have documented coherence between these two properties in several different regions of the world ocean, including the northeast Atlantic (Gower et al., 1980), the California Current (Smith et al., 1988; Denman and Abbott, 1994; Abbott and Letelier, 1998) and the Gulf Stream (Garcia-Moliner and Yoder, 1994). However, the nature of this relationship in the oligotrophic regions of the main subtropical gyres has received less attention, perhaps owing to the weaker signals in those areas. The objectives here are threefold: (1) to determine the nature of the mesoscale signal in ocean color and SST distributions in the Sargasso Sea, (2) to ascertain the degree to which they are linked, and (3) to understand the information this provides about the role of mesoscale processes in shaping upper ocean plankton distributions and the implications for biogeochemical cycling.

2. Methods

The study domain is a $6 \times 6^{\circ}$ region of the Sargasso Sea, centered at 29°N, 70°W (Fig. 1). It was chosen to coincide with domains of the MODE and POLYMODE programs, for which the most robust eddy statistics are available (e.g., Richman et al., 1977; The MODE Group, 1978). Using the CZCS browse archive (Feldman et al., 1989), all imagery containing pigment data within the study domain was identified. A subset of these CZCS images was selected based on simultaneous

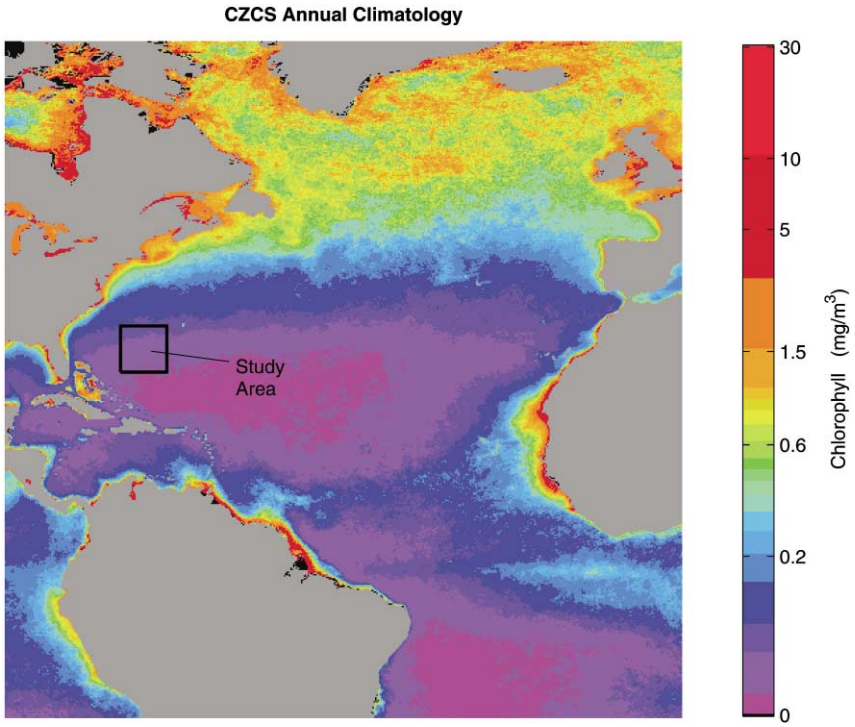

Fig. 1. Composite of all Nimbus-7 Coastal Zone Color Scanner data collected in the North Atlantic (November 1978 through June 1986). The box in the Sargasso Sea indicates the region in which high-resolution individual images are analyzed, and monthly composites were extracted from SST and ocean-color archives.

(same-day) availability of SST imagery. This subset of the CZCS archive was acquired at full resolution ($\sim 1 \times 1$ km) from NASA/Goddard Space Flight Center. Data were processed from level 1 (top of the atmosphere radiance) to level 3 (standard map projection) pigment fields using the clear-water atmospheric correction algorithm (Gordon and Clark, 1981) and a 3-band pigment algorithm (Clark, 1981). For atmospheric correction of the CZCS imagery, aerosol optical thickness ratios for typical marine aerosols were used. Cloud pixels were removed from AVHRR images using a manual declouding program in which a threshold temperature is specified (clouds being cold relative to SST).

During the 8-year lifetime of the CZCS instrument, there were 21 days in which simultaneous SST and ocean-color imagery were available over significant portions of the mapping domain. The relative paucity of suitable image pairs in this region stems from (1) the open ocean was not the primary target of the CZCS mission, and (2) cloudiness frequently obscured the instrument's field of view. Subsequent ocean-color missions such as SeaWiFS will provide more regular coverage of the open ocean, but cloudiness remains the central issue. Compositing time series of partially clear images provides one approach to dealing with the cloudiness problem, but it has the disadvantage of space/time smearing. Because the present focus on mesoscale structure requires synoptic measurements, a compositing strategy was not pursued. Thus the 21 pairs of simultaneous images form the basis of this study.

The seasonal distribution of the image pairs is strongly skewed toward winter and spring; very few are available in the summer and fall (see below). In order to place the high-resolution results into their seasonal context, it is necessary to rely on data sets that are appropriately averaged in space and time. For these purposes, monthly composites were extracted from the Global CZCS archive (18 km nominal resolution) at NASA/Goddard Space Flight Center (see http://seawifs.gsfc.nasa.gov/ SEAWIFS/IMAGES/CZCS_DATA.html). Corresponding archives of composited SST data available to date do not completely overlap with the CZCS mission in terms of their temporal coverage. Several products are available; we chose to use the NOAA/NASA AVHRR Oceans Pathfinder archive (see http://podaac.jpl.nasa.gov/sst). Monthly composites of night-time SST images in the study domain were extracted from the global 9-km data base that spans the years 1987–1993.

3. Results

High-resolution imagery reveals clear mesoscale signals in both SST and ocean color. All 21 pairs of SST and ocean-color images are available for inspection in both graphical and raw forms on the enclosed CD-ROM and also on the world wide web at http://science.whoi.edu/users/mcgillic/czcs-avhrr/. Two sets of example images are shown in Fig. 2. On April 20, 1984, a pair of eddies with cold SST anomalies are oriented northwest–southeast (panel (a), features 1 and 2). The SST pattern in eddy 2 suggests cyclonic rotation, with a tongue of warm water apparently being drawn around the north flank of the feature. The sense of rotation in eddy 1 is less clear, although the tendril of cold water extending north and west from its northeast corner hints it is an anticyclone. Generally speaking, pigment patterns show a strong inverse relationship with SST. Very low pigment concentrations are present in waters warmer than 22°C; values are at or below the limit of detection (0.04 mg Chl-a m^{-3}) in the broad area south, east and west of the eddy pair. Pigment concentration within the two eddies is elevated above the background by a factor of two or more. High pigment values are also associated with the large area of relatively cool water to the east of the eddy pair.

Eight days later, the two eddies are still the most prominent features in the area (Fig. 2b). The SST image suggests the center of eddy 1 has translated approximately 30 km to the northwest, while the center of eddy 2 has moved about 30 km to the south–southwest. Although changes in shapes of the eddies contribute some uncertainty to these estimates of displacement, the inferred propagation speeds of approximately 4 km day^{-1} are consistent with those observed in this region during the MODE and POLYMODE programs (Richman et al., 1977; The MODE Group, 1978). Eddy 1's anticyclonic rotation is much more evident in this later image: two tendrils of cooler water extend southward from the western flank of the eddy, wrapping eastward around the southern portion of the feature. It is entirely possible that these streamers are the same as those observed to the north of the eddy on April 20. A typical swirl velocity of 20 cm s^{-1} (Richman et al., 1977; The MODE Group, 1978) would result in a rotation period of approximately 2 weeks. In this case, the streamers appear to have gone half-way around in 1 week. Overall, pigment concentration has increased modestly. The two eddies are still clearly visible as biomass maxima, as is the large area of low SST, high-pigment water to the east. Again, waters warmer than about 22°C have generally lower pigment, as is the case over much of the southeast quadrant of the image. The same does not

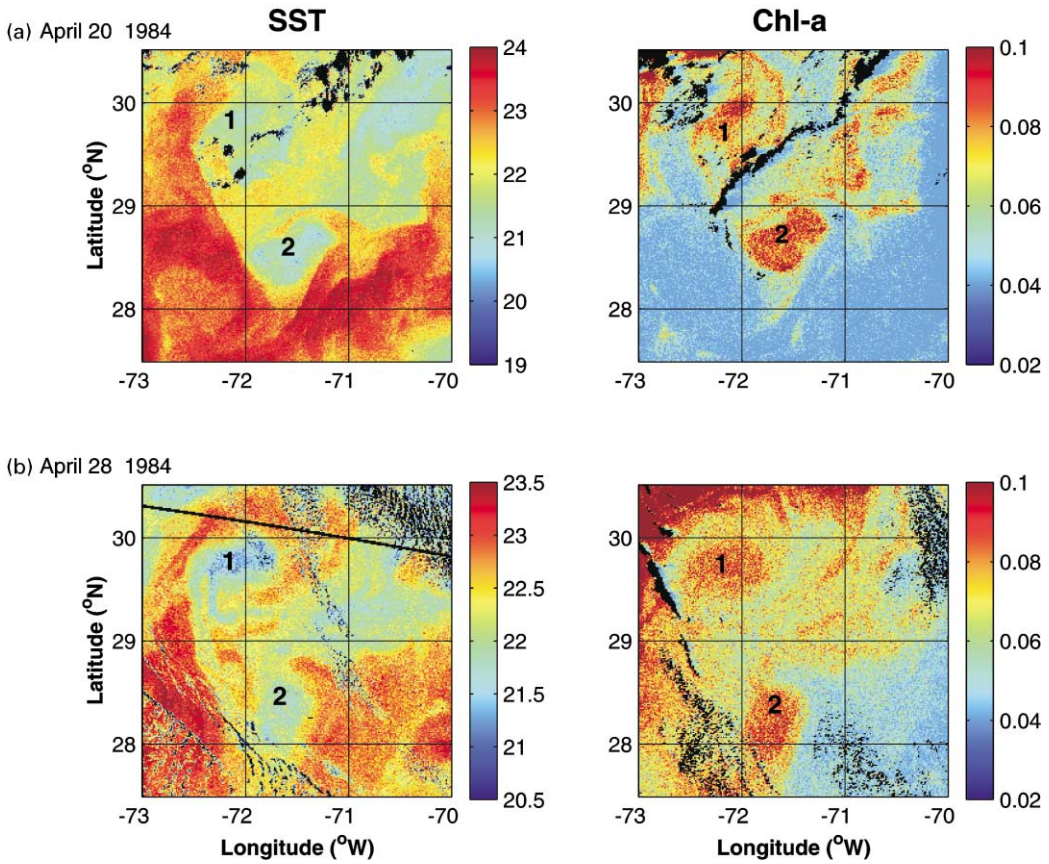

Fig. 2. Simultaneous sea-surface temperature and ocean-color images from (a) April 20, 1984, and (b) April 28, 1984. Note that the domains shown here are zoomed-in subregions of the box depicted in Fig. 1. Pixels identified as clouds appear black. Numerals identify eddy features described in detail in the text. Note that the color bar extends slightly below the noise floor of the measurement (0.04) simply for clarity of presentation.

appear to be true in the southwest quadrant, as it was before on April 20 (panel [a]). However, this apparent inconsistency is in an area of scattered cloud cover, and its interpretation is therefore suspected. The broad area of high pigment in the northwest corner of the map is also suspicious; the full image reveals this may be a result of aerosol contamination.

The strong mesoscale content in SST and surface-pigment variations contained in these images is characteristic of the entire data set. In order to provide a quantitative statistical measure of the dominant spatial scales inherent in the data, the autocorrelation functions for both SST and surface pigment were computed for each image. Linear trends in both zonal and meridional directions were subtracted prior to these calculations to remove the large-scale gradients. Zero-crossings of the autocorrelation functions for both SST and surface pigment occur at distance lags consistent with mesoscale phenomena (Fig. 3). Zonal scales in SST and surface pigment are nearly identical (135 and 137 km, respectively). Meridional scales are about 20% larger, ranging from 160 km for SST to 176 km for surface pigment. As there is no evidence for such anisotropy in the mesoscale fields

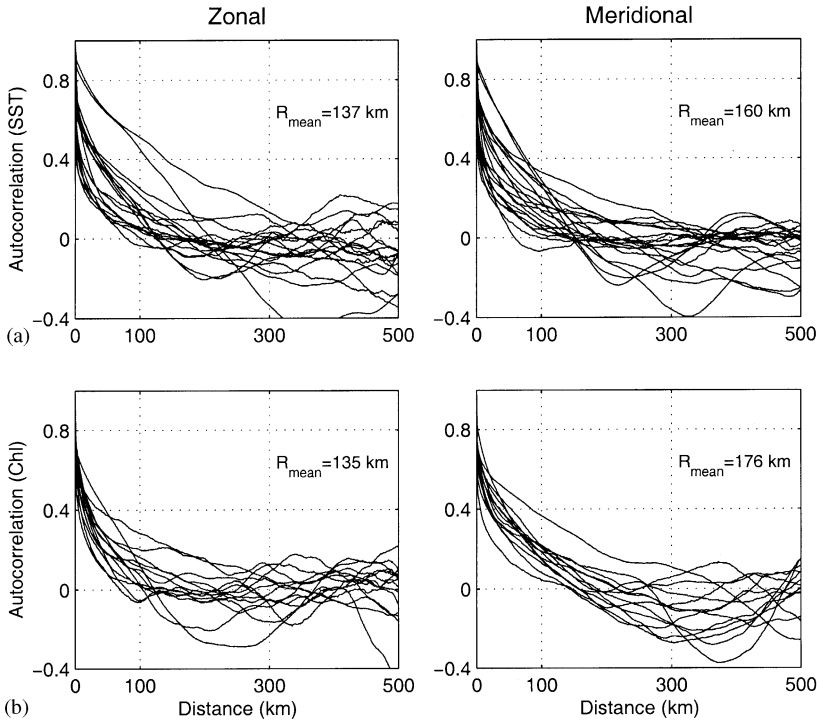

Fig. 3. Spatial autocorrelation of (a) sea-surface temperature, and (b) surface pigment in the zonal (left-hand column) and meridional (right-hand column) directions. Each line represents the computation performed on an individual high-resolution image, with linear trends removed in both directions. The distance R_{mean} in each plot refers to the average zero crossing for all images in which the first zero crossing was less than 200 km.

themselves, this suggests that a portion of the large-scale meridional gradient remained subsequent to removal of the linear trend.

Covariation between SST and surface pigment is also a consistent feature of the data set (Fig. 4). In this figure, two estimates of the statistical significance of the correlations are provided. Under the assumption that each pixel represents an independent measurement, the 95% confidence intervals are scarcely larger than the plot marks (dots) themselves. A more conservative estimate of the number of degrees of freedom would be to assume that pixels within a Rossby radius of each other are not independent (this radius represents scale at which the geostrophic balance characteristic of mesoscale eddy dynamics becomes relevant). Using a Rossby radius of 45 km in this region, there are 225 degrees of freedom in the typical image. This yields a critical magnitude for correlations of 0.1 (indicated by the dotted lines in Fig. 4), above which they are significantly different from zero at the 95% confidence level. In only one instance is there positive correlation between SST and surface pigment; in all other cases the correlation is negative (or not significantly different from zero using the more strict statistical criterion), such that cold (warm) SST anomalies correspond to high (low) biomass, as in Fig. 2. Although only a portion of the year is adequately resolved in the composite time series, there does appear to be a significant ($r^2 = 0.37$) seasonal trend during that

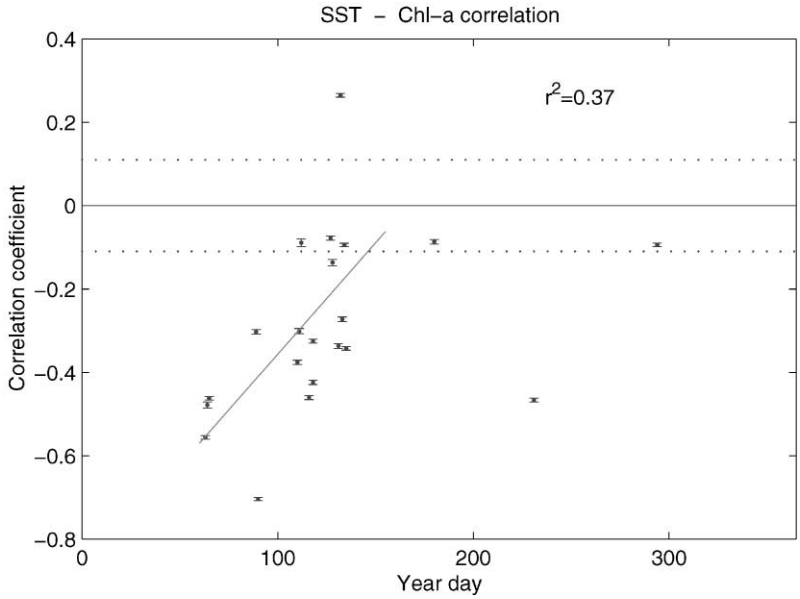

Fig. 4. Correlation between sea-surface temperature and surface pigment for the 21 pairs of simultaneous (same-day) images. The correlation coefficient is plotted as a function of year day in a composite year. Vertical bars indicate the 95% confidence interval for the correlation estimate assuming the number of degrees of freedom is equal to the number of cloud-free pixels in each image pair. The dotted line represents a more conservative estimate of the statistical significance of the correlations in which the number of degrees of freedom is based on the Rossby radius of deformation for the region (see text). The solid line is a least-squares fit to the points in the portion of the year which is adequately resolved (year days 0–150), for which $r^2 = 0.37$.

time interval (year days 0–150). The strongest correlation occurs during winter, and weakens as the year progresses toward summer.

It is unfortunate that only about half of the annual cycle is resolved by the time series of simultaneous high-resolution SST and ocean-color images. Statistics of monthly composite SST and ocean-color images help put this information into its seasonal context (Fig. 5). The mean values of both SST and surface pigment have a strong seasonal cycle, as well as significant interannual variability. The same is also true of the variance. Interestingly, in both cases the highest variance occurs during the winter, when SST is coldest and biomass at its highest. Conversely during summer, when SST is warmest and biomass is lowest, both quantities have minimum variance. Thus, the seasonal trend in correlation between SST and surface pigment observed in the high-resolution imagery (Fig. 4) coincides with a trend of decreasing variance in both quantities.

What is the cause of this seasonal cycle in variance? The total variance plotted in Fig. 5 includes contributions from both the large-scale gradients and the mesoscale signal. These seasonal variations could arise from fluctuations in the magnitude of the large-scale gradients, changes in the strength of the mesoscale contribution to the total variance, or both. Statistics of the monthly composite images offer a means to distinguish between the two. Linear trends in the zonal and meridional directions provide an estimate of the large-scale gradients (Fig. 6). There is little seasonality in the zonal trends of SST and surface pigment. However, a noticeable seasonal

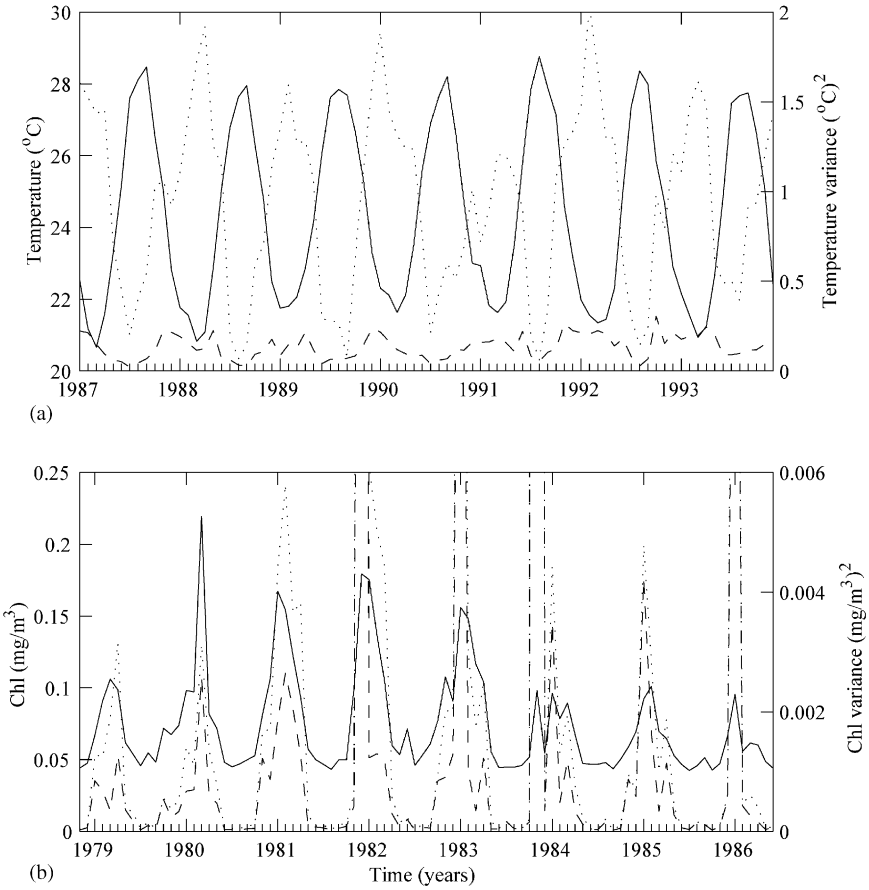

Fig. 5. Statistics from monthly composite images in the study region shown in Fig. 1 (a) SST from the NOAA/NASA AVHRR Oceans Pathfinder 9 km data, and (b) surface pigment from the NASA/Goddard Global CZCS archive (18 km). Solid line: mean value; dotted line: total variance; dashed line: variance of detrended data (see text).

modulation of the meridional trends exists in both quantities: north–south gradients are maximum in winter and decrease toward summer. This suggests large-scale meridional gradients contribute to the observed seasonal cycle in variance.

Does the mesoscale contribution to surface property distributions vary seasonally? The variance of the residuals of these detrended monthly composites provides a clue, with one important caveat: monthly compositing tends to smear out mesoscale features. Thus, the variance of the detrended fields should be related to the magnitude of the mesoscale signal, but perhaps biased toward the lower end of the true mesoscale variance. The fraction of the total variance remaining after detrending (the "eddy variance") varies considerably (Fig. 5). In general, the eddy variance is a much larger fraction of the total variance in surface pigment (64%) than SST (18%). Seasonal variations in SST total variance are dominated by the large-scale gradients, which are at their maximum in winter. As the year progresses, the large-scale gradients diminish such that the remaining variance is mostly mesoscale. Note that the eddy variance in SST does vary seasonally,

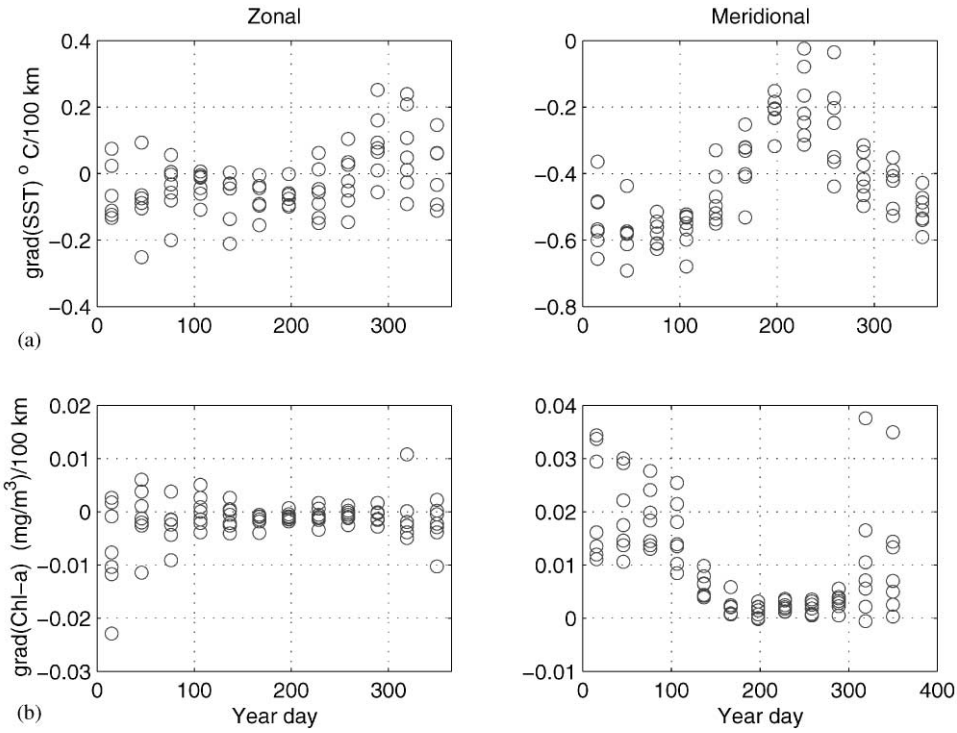

Fig. 6. Zonal and meridional gradients computed from monthly composite images in the study region shown in Fig. 1 (a) SST from NOAA/NASA AVHRR Oceans Pathfinder 9 km data, and (b) surface pigment from the NASA/Goddard Global CZCS archive (18 km).

generally reaching its maximum in winter and minimum in summer. Partitioning of the surface-pigment variance is quite different: the eddy contribution makes up a much larger fraction of the total, dominating the seasonal cycle in variance. This seasonality in both SST and surface-pigment variance suggests there may be time dependence in the magnitude of the mesoscale contribution to the overall property distributions.

It is of interest to determine the degree to which the covariation of SST and surface pigment shown in Fig. 4 is influenced by seasonal effects. Correlations between image pairs were thus recomputed after removal of linear trends in both zonal and meridional directions. This resulted in an overall decrease in the magnitude of the correlations as compared with the prior case (Fig. 7). Although the correlations are significant in all but two cases assuming each pixel is independent, only about half of them are significant when the more conservative estimate of the number of degrees of freedom is used. Nevertheless, the mean correlation value for all image pairs (-0.11) is significant at the 95% confidence level even for the more stringent error criterion. Note that there is no significant seasonal variation in the amplitude of the correlation coefficient computed from the detrended images. Thus it appears that the seasonal signal evident in the covariation of the raw data (Fig. 4) results from large-scale gradients rather than mesoscale phenomenology.

It could be argued that a more appropriate approach to removal of the large-scale gradients from the synoptic imagery would rely on climatological observations rather than the individual

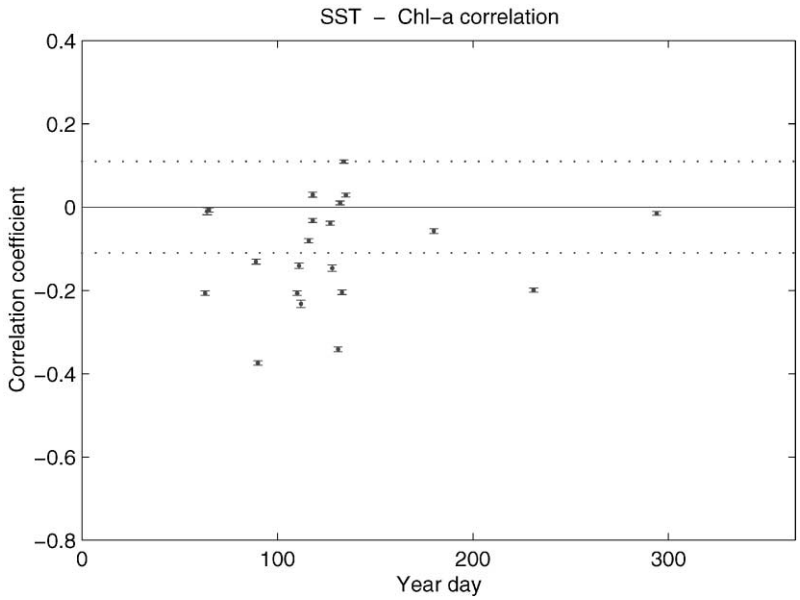

Fig. 7. Correlation between sea-surface temperature and surface pigment for the 21 pairs of simultaneous images. Linear trends in both zonal and meridional directions are removed from each image prior to computing the correlations. The correlation coefficient is plotted as a function of year day in a composite year. Two estimates of confidence intervals for the correlations are shown, as in Fig. 4.

images themselves. To investigate this possibility, linear trends derived from monthly climatologies of the AVHRR and CZCS data were removed from each individual image. The resulting set of correlation coefficients for the 21 image pairs contained an even stronger seasonal signal than those computed from the raw data (not shown). Hence, residual trends from interannual variations in the large-scale gradients must contribute to the correlation estimates. Therefore, we conclude that the preferred method for exposing the correlation between mesoscale variations in SST and surface pigment is the removal of linear trends from each individual image, as in Fig. 7. The results of that computation indicate that the correlation coefficient is negative in nearly every case, with a mean value of -0.11.

4. Discussion

4.1. Spatial correlation scales

The spatial scales characteristic of AVHRR and ocean-color imagery computed here are similar to those found elsewhere in the North Atlantic. On the basis of four cloud-free CZCS images in the vicinity of 47°N, 20°W (the site of the JGOFS North Atlantic Bloom Experiment) Robinson et al. (1993) calculated a mean length scale of 160 km (range 90–320 km) for surface-pigment distributions. Yoder et al. (1993) documented a coincidence in SST and surface-pigment scales (similar to that reported herein) using Airborne Oceanographic Lidar (AOL). Although the mean lengths they

calculated are shorter (59 and 49 km, respectively), the range encompasses those identified in the present study.

4.2. Covariation of ocean color and SST

The preceding analysis reveals an inverse relationship between mesoscale SST and surface pigment variations, such that cold (warm) temperature anomalies are associated with high (low) pigment biomass. Although this is a consistent pattern in the observations, the correlation coefficients are generally low, with an average of -0.11. How does this compare to what might be expected given the physical–biological interactions thought to be responsible for generating these patterns in the Sargasso Sea? In general, only a portion of this region — perhaps 30% (Koshlyakov, 1986) — will be occupied by eddies at any one time. Assuming an equal number of warm and cold eddy-driven SST anomalies (we are not aware of any evidence this is not the case in the Sargasso Sea), we infer that 15% of the total area contains eddy-driven SST anomalies that are cold, and 15% warm. [Note that there are at least two different types of eddies in the Sargasso Sea that can give rise to cold SST anomalies: typical mid-ocean cyclones and mode-water eddies (which are anticyclones). For a more complete discussion, see McGillicuddy et al. (1999)]. If the biomass response to both warm and cold features were perfectly linear, then an average correlation coefficient of 0.3 would be expected. However, there are several aspects of the underlying mechanisms which are highly nonlinear. To begin with, the biological ramifications of eddy-induced isopycnal displacements are not symmetric [MR97]. Upwelling in the interiors of cold features introduces nutrients into the euphotic zone, which stimulates biomass accumulation. In contrast, there is little stimulus for a biological response in the warm eddy case: downwelling simply forces nutrient-depleted water out of the euphotic zone. There is evidence in the imagery presented here as well as some in situ observations (McGillicuddy et al., 1999) that such warm features are impoverished with respect to the background biomass. However, the sense of the vertical nutrient gradient in oligotrophic waters clearly sets the stage for an asymmetric biological response to vertical isopycnal displacements: upwelling leads to enhanced phytoplankton growth, while downwelling does not.

There are also aspects of the temporal dynamics of eddies that could potentially impact the magnitude of the correlation between SST and surface-pigment distributions. Eddies can change a great deal during their lifetimes, which can last several months to in excess of 1 year in this region (Richardson, 1993). Whether a particular eddy is forming, interacting with surrounding features, or decaying will determine the changes in isopycnal displacements that are occurring at any one time. The sense of these perturbations could have fundamental impacts on the biological response. For example, it is only during the formation and intensification of cold eddies that new nutrients are introduced into the euphotic zone; as the feature decays the isopycnal surfaces relax to their unperturbed state, causing downwelling. It is therefore possible that strong correlation between physical and biological variables within an eddy would persist only during certain portions of its lifetime. This too would tend to decrease the average value of the correlation coefficient.

Precision of the ocean-color sensor is also an issue. Pigment concentrations in the Sargasso Sea are much lower than the areas for which the instrument was designed, and many pixels are reported at its threshold for detection (0.04 mg pigment m^{-3}). Truncation of the lowest biomass values

at this threshold value also could reduce the average correlation, because the full dynamic range of pigment variations in the Sargasso Sea was not resolved by the sensor.

4.3. What is the ocean-color signal?

Although the terms ocean color, pigment, and biomass have been used interchangeably here, it is well known that the spectral resolution of the CZCS instrument was not sufficient to separate out colored detrital materials (CDM), either dissolved or particulate. High-quality bio-optical measurements from the Bermuda Bio-optical Program (BBOP) have revealed concentrations of CDM that are sufficient to cause attenuation that is significant with respect to the magnitude of the pigment-containing signal (Siegel et al., 1995; Siegel and Michaels, 1996; Nelson et al., 1998). Thus it is likely that pigment estimates derived from CZCS measurements reflect some combination of pigments and CDM. Without additional data, it is not possible to determine the partitioning between the two. However, mesoscale biogeochemical surveys have revealed significant chlorophyll variations associated with eddies that are similar in pattern to that observed in the satellite images presented herein. McGillicuddy et al. (1999) document enhanced (reduced) chlorophyll concentrations overlying eddies which displace isopycnals upward (downward). Although they present a spatial map of chlorophyll at the 60 m depth horizon only, similar patterns exist in the top few optical depths. Therefore it seems likely that a significant portion of the mesoscale patterns in surface ocean color derived from CZCS observations are associated with plant pigments.

4.4. Passive tracer or biological response?

It is important to realize that the mesoscale variations in SST and ocean color described here do not necessarily imply a biological response to eddy-driven nutrient injection. Near-surface gradients in nutrients, chlorophyll and CDM all have the same sense in this region of the ocean. During most of the year, nitrate is depleted down to 80–90 m, at which depth the concentration begins to increase rapidly (Michaels et al., 1994). Typical chlorophyll profiles contain a subsurface maximum that resides at the top of the nitracline (Michaels et al., 1994). Profiles of CDM show a similar vertical structure (except during periods of wintertime convection), with the subsurface maximum residing slightly shallower than that of chlorophyll (Siegel and Michaels, 1996; Nelson et al., 1998). This alignment of the vertical gradients in all three properties suggest that eddy-induced upwelling of nutrients also would tend to introduce higher concentrations of both pigments and CDM into the surface layers. Thus, the decrease in water clarity observed in the interiors of upwelling features could be a complex combination of (1) biomass enhancement stimulated by the introduction of nutrients into the euphotic zone, and (2) vertical advection of colored materials (both chlorophyll and CDM) from their subsurface maxima. Without direct measurements of biological rates associated with the mesoscale property distributions, it is not possible to distinguish between the two quantitatively. However, Siegel and Michaels (1996) did attempt to quantify the error in CZCS chlorophyll retrievals caused by CDM. Their estimate was on the order of 0.025 mg m^{-3} Chl-*a*. Given that the magnitude of the mesoscale variations are four times larger than this, it is unlikely that CDM can fully explain the observed ocean-color signal. Thus, a significant biological response is clearly implied.

5. Conclusions

The ensemble of 21 pairs of CZCS and AVHRR images presented here are replete with mesoscale phenomenology. The spatial scales present in both ocean color and SST coincide with the 100–150 km dimensions typical of mesoscale eddies in the region. The two properties covary inversely ($r^2 = -0.11$), such that cold (warm) temperature anomalies are associated with high (low) concentrations of colored materials. The general sense of this relationship is consistent with the notion of eddy-induced nutrient transport stimulating biological productivity in the Sargasso Sea (MR97; McGillicuddy et al., 1998; Siegel et al., 1999). Furthermore, the magnitude of the cross-correlation is similar to what one would expect given the nature of the physical–biological interaction, demographics of eddies in the region, and limitations of the ocean-color instrument. However, it is important to point out that these patterns would tend to be reinforced by the accompanying vertical advection of colored materials, including both plant pigments and CDM. Quantitative discrimination between such passive advection and the biological response to nutrient injection will require simultaneous assessment of biological rates as well as property distributions. Due to the spatial and temporal intermittency of the attendant processes, an integrated approach consisting of remote sensing, in situ observations, and data-assimilative numerical modeling will be necessary to adequately resolve such phenomena. Recent progress towards concurrent operation of a full complement of remote sensors (SST, ocean color, altimetry, winds) will help provide a more complete observational basis for future studies of this type.

Acknowledgements

The support of this research by JPL, NASA and NSF is gratefully acknowledged. Special thanks to Olga Kosnyreva who contributed a great deal to data processing and graphical presentation. Norm Nelson and Tommy Dickey are thanked for their reviews, which helped improve the manuscript. This is WHOI contribution 9892, and US JGOFS contribution 542.

References

Abbott, M., Letelier, R.M., 1998. Decorrelation scale of chlorophyll as observed from bio-optical drifters in the California Current. Deep-Sea Research II 45, 1639–1667.

Clark, D., 1981. Phytoplankton algorithms for the Nimbus-7 CZCS. In: Gower, J.F.R. (Ed.), Oceanography from Space. Plenum Press, New York, pp. 227–238.

Denman, K., Abbott, M.R., 1994. Time scales pattern evolution from cross-spectrum analysis of advanced very high resolution radiometer and coastal zone color scanner imagery. Journal of Geophysical Research 99, 7433–7442.

Dickey, T., Frye, D., Jannasch, H., Boyle, E., Manov, D., Sigurdson, D., McNeil, J., Stramska, M., Michaels, A.F., Nelson, N., Siegel, D.A., Chang, G., Wu, J., Knap, A.H., 1998. Initial results from the Bermuda Testbed Mooring program. Deep-Sea Research I 45, 771–794.

Doney, S., 1996. A synoptic atmospheric surface forcing data set and physical upper ocean model for the US JGOFS Bermuda Atlantic Time Series (BATS) site. Journal of Geophysical Research 101, 25 615–25 634.

Feldman, G., Kuring, N., Ng, C., Esaias, W., McClain, C., Elrod, J., Maynard, N., Endres, D., Evans, R., Brown, J., Walsh, S., Carle, M., Podesta, G., 1989. Ocean color: availability of the global data set. EOS Transactions 70 (23), 634–635, 640–641.

Garcia-Moliner, G., Yoder, J.A., 1994. Variability in pigment concentration in warm-core rings as determined by coastal zone color scanner satellite imagery from the Mid-Atlantic Bight. Journal of Geophysical Research 99, 14 277–14 290.

Gordon, H.R., Clark, D.K., 1981. Clear water radiances for atmospheric correction of Coastal Zone Color Scanner imagery. Applied Optics 20, 4175–4180.

Gower, J., Denman, K.L., Holyer, R.J., 1980. Phytoplankton patchiness indicates the fluctuation spectrum of mesoscale oceanic structure. Nature 288, 157–159.

Jenkins, W., 1988. The use of anthropogenic tritium and helium-3 to study subtropical gyre ventilation and circulation. Philosophical Transactions of the Royal Society 325, 43–61.

Koshlyakov, M., 1986. Eddies in the open ocean. In: Kamenkovich, V., Koshlyakov, M.N., Monin, A.S. (Eds.), Synoptic Eddies in the Ocean. D. Reidel Publishing Company, Dordrecht, pp. 265–376.

McGillicuddy, D., Johnson, R., Siegel, D.A., Michaels, A.F., Bates, N.R., Knap, A.H., 1999. Mesoscale variations of biogeochemical properties in the Sargasso Sea. Journal of Geophysical Research 104, 13 381–13 394.

McGillicuddy, D., Robinson, A.R., 1997. Eddy induced nutrient supply and new production in the Sargasso Sea. Deep-Sea Research I 44, 1427–1449.

McGillicuddy, D., Robinson, A.R., Siegel, D.A., Jannasch, H.W., Johnson, R., Dickey, T.D., McNeil, J., Michaels, A.F., Knap, A.H., 1998. Influence of mesoscale eddies on new production in the Sargasso Sea. Nature 394, 263–265.

McNeil, J., Jannasch, H.W., Dickey, T.D., McGillicuddy, D.J., Brzezinski, M., Sakamoto, C.M., 1999. New chemical, bio-optical and physical observations of upper ocean response to the passage of a mesoscale eddy. Journal of Geophysical Research 104, 15 537–15 548.

Michaels, A.F., Knap, A.H., Dow, R.L., Gundersen, K., Johnson, R.J., Sorenson, J., Close, A., Knaver, G.A., Lohrenz, S.E., Asper, V.A., Tuel, M., Bidigare, R., 1994. Seasonal patterns of Ocean biogeochemistry at the US JGOFS Bermuda Atlantic Time-series Study site. Deep-Sea Research I 41, 1013–1038.

Nelson, N., Siegel, D.A., Michaels, A.F., 1998. Seasonal dynamics of colored dissolved material in the Sargasso Sea. Deep-Sea Research I 45, 931–957.

Richardson, P., 1993. A census of eddies observed in North Atlantic SOFAR float data. Progress in Oceanography 31, 1–50.

Richman, J., Wunsch, C., Hogg, N.G., 1977. Space and time scales of mesoscale motion in the Western North Atlantic. Reviews of Geophysics and Space Physics 15, 385–420.

Robinson, A., McGillicuddy, D.J., Calman, J., Ducklow, H.W., Fasham, M.J.R., Hoge, F.E., Leslie, W.G., McCarthy, J.J., Podewski, S., Porter, D.L., Saure, G., Yoder, J.A., 1993. Mesoscale and upper ocean variabilities during the 1989 JGOFS bloom study. Deep-Sea Research II 40, 9–35.

Siegel, D., McGillicuddy, D.J., Fields, E.A., 1999. Mesoscale eddies, satellite altimetry and new production in the Sargasso Sea. Journal of Geophysical Research 104, 13 359–13 379.

Siegel, D., Michaels, A.F., 1996. Quantification of non-algal light attenuation in the Sargasso Sea: implications for biogeochemistry and remote sensing. Deep-Sea Research II 43, 321–345.

Siegel, D., Michaels, A.F., Sorenson, J.C., O'Brien, M.C., Hammer, M.A., 1995. Seasonal variability of light availability and utilization in the Sargasso Sea. Journal of Geophysical Research 100, 8695–8713.

Smith, R., Zhang, X., Michaelson, J., 1988. Variability of pigment biomass in the California Current System as determined by satellite imagery, Part 1. Spatial variability. Journal of Geophysical Research 93, 10 863–10 882.

The MODE Group, 1978. The Mid-Ocean Dynamics Experiment. Deep-Sea Research 25, 859–910.

Yoder, J., Aiken, J., Swift, R.N., Hoge, F.E., Stegmann, P.M., 1993. Spatial variability in near-surface chlorophyll *a* fluorescence measured by the airborne oceanographic lidar (AOL). Deep-Sea Research II 40, 37–54.